Sliding Mode Control for Wind Turbine with Doubly Fed Induction Generators

Watthana Seubkinorn and Bunlung Neammanee

Abstract*— *The main objective of a wind energy conversion system is to converse energy from the wind into electrical energy as much as possible. The power coefficient characteristic of a wind turbine has a single maximum at a specific value of the tip speed ratio. The wind turbine should, therefore, operate at the maximum power coefficient. Another important objective for wind turbine operation is to limit the output at the rated value. The paper presents a wind turbine control technique based on a sliding mode control (SMC) for the two control objectives. The simulation result from a case study shows that the SMC has good tracking performance and it can efficiently regulate the maximum peak power.

***Keywords*— Sliding mode control, wind turbine, doubly fed induction generator.**

1. INTRODUCTION

Wind turbines are generally composed of a rotating rotor with three blades. This rotor is the aerodynamic component of the wind turbine. It captures the energy available in the wind, and transfers it to a rotating shaft, located inside the wind turbine nacelle. The shaft is mechanically connected to the electromechanical converter unit. The main objective of a wind energy conversion system is to converse energy from wind into electrical energy with maximum efficiency. The power coefficient characteristic of a wind turbine has a single maximum at a specific value of the tip speed ratio. The wind turbine should, therefore, operate at the optimum power coefficient.

In this paper, the electromechanical converter unit is a gearbox with a doubly fed induction generator (DFIG) shown in Figure 1. The stator winding of the DFIG is directly connected to the grid and its wound rotor is connected with a static Kramer drive. The static Kramer drive topologies have a three phase diode bridge rectifier located in machine side, and a three phase line commutate thyristor inverter are located in line side. The rectifier and inverter are coupled together with an inductor. Power flow can be controlled from the rotor circuit by commanding the firing angle of the thyristor unit in a range between 90 and 180 degrees to be operated in inverting mode. The rotational speed of the rotor must be higher than synchronous speed or operates only at supersynchronous speed to generate electrical power from both the stator and the rotor circuits.

Operating regions is generally classified into four regions as shown in Figure 2, which represents a typical power versus wind speed curve of a wind turbine. The figure indicates three wind velocities on which the four regions are separated based. In the figure, the cut-in velocity is defined as the wind speed at which the turbine starts to generate the power. Below this wind speed, it is not efficient to turn on the turbine. The rated velocity (v_{rated}) is the wind speed at which the turbine reaches its rated turbine power. The cut-out velocity ($v_{cut-out}$) is the maximum wind speed at which the wind turbine can still operate. Beyond this wind speed, the rotor has to be shut down to keep the blades, the electrical generator and other components from reaching damaging level [3-4].

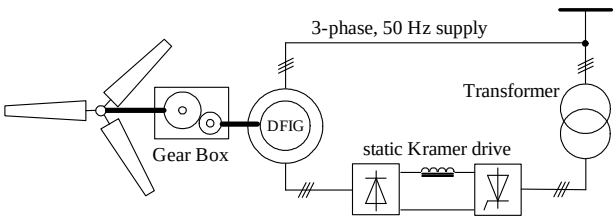

Fig. 1. Schematic diagram of WECS by DFIG with static Kramer drive system.

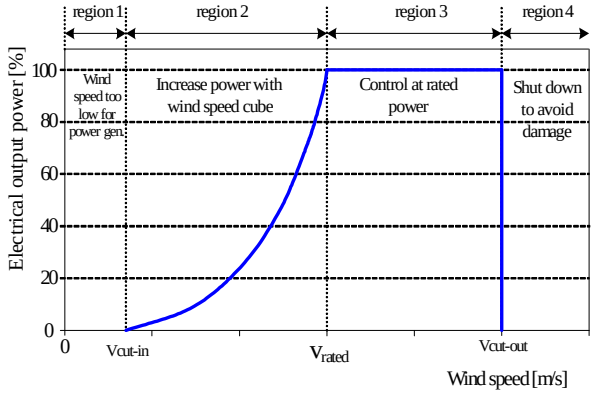

Fig. 2. Operation area of wind turbine.

The operation regions of interest in this paper are regions 2 and 3. Region 2 covers a wind speed range between v_{cut-in} and v_{rated} and is referred as the below rated power region. Because the power generated from a

The authors are with Department of Electrical Engineering, King Mongkut's University of Technology North Bangkok 1518 Bangsue, Bangkok 10800, Thailand. Phone: (+66)2913-2500-24 Ext: 8420; Fax: (+66)2585-7350; E-mail: bln@kmutnb.ac.th, wsk@sau.ac.th.

wind speed in this region is a function of the cube of that wind speed, the main task of a controller is to capture the maximum power output for that wind speed. Region 3 covers a wind speed range between v_{rated} and $v_{cut-out}$ and is referred as the above rated power region. As the mechanical power generated by the rotor is limited, the main task of a controller in this region is to keep output at its rated power [4].

This paper presents a sliding mode control (SMC) developed with a designed control law to force the generator torque to be a linear function of the generator speed around the operating point of maximum power transfer in the below rated wind speed region. In addition, the power is limited by stall regulation in the above rated wind speed region.

2. MATHAMATICAL MODEL OF SYSTEM

The mathematical model of wind turbine is described in section 2.1. The mathematical model of the static Kramer drive and the DFIG are described in section 2.2. Section 2.3 presents the overall system that combines sections 2.1 and 2.2.

2.1. Mathematical Model of Wind Turbine

The power generated from the wind can be expressed by (1). According to Betz's law, an ideal wind turbine would, in theory, extract the 16/27 of this power. However, in practice, due to non-laminar air flow and friction between blade surfaces, the energy capture of the wind turbine is reduced by a factor known as the power coefficient, c_P, given in (2). Another two important characteristics of the wind turbine are the torque coefficient and aerodynamic torque defined in (5).

$$P_w = \frac{1}{2}\rho A v^3 \tag{1}$$

$$c_P(\lambda) = \frac{P_{\text{rotor}}}{P_{\text{wind}}} = \frac{P_{\text{rotor}}}{1/2\rho A v^3} \tag{2}$$

where

$$P_{rotor} = \frac{1}{2}\rho A v^3 c_P(\lambda) \tag{3}$$

$$\lambda = \frac{R\Omega}{v} \tag{4}$$

$$T_a = \frac{1}{2}\rho\pi R^3 v^2 c_T(\lambda) \tag{5}$$

where

$$c_T = \frac{c_P}{\lambda} \tag{6}$$

The main control objective is to maximize energy capture from the wind. Each wind turbine has its own power and torque characteristics. Figure 3 is an example of wind turbine characteristics. As can be seen, the turbine has a single maximum power coefficient, $c_P^{\max}$, at the tip speed ratio λ_0. When the rotor operates at constant speed, the power coefficient will be at maximum at only one wind speed and therefore to achieve the highest annual energy capture. The value of the power coefficient must be maintained at the maximum level all the time [1, 2].

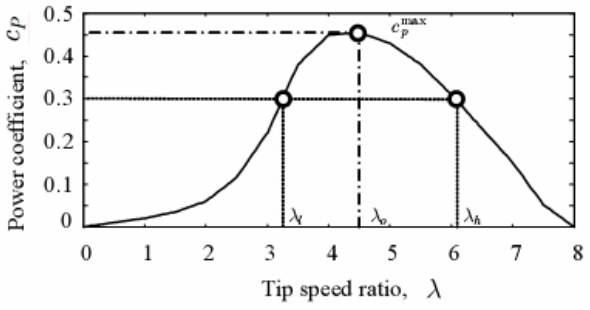

Fig. 3. Power coefficient curve, c_P, versus TSR, λ

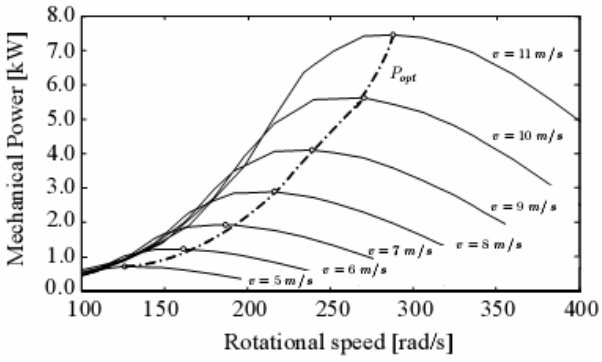

Fig. 4. Aerodynamic power versus rotational speed of generator shaft for various wind velocities.

Figure 4 shows a power-rotational speed curve with seven different wind speeds (5, 6, ..., 11 m/s). Path P_{opt} in the figure indicates the optimum tracking path on which each operating point has $c_P^{\max}$.

2.2. Mathematical Model of DFIG and Static Kramer Drive

Figure 5 shows a per phase equivalent circuit of the DFIG with the static Kramer drive in Figure 1 to analyze electrical power production from mechanical power. The generator torque can be calculated using (7) [2, 6]. The cosine value of firing angle, cos(α), commands the thyristor unit and the rotational speed , Ω, of the DFIG.

$$T_g(\cos\alpha, \Omega) = \frac{3V_s^2 sR_{EQ}(\cos\alpha)\Omega_s^{-1}}{(sR_s + R_{EQ}(\cos\alpha))^2 + (s\omega_s(L_{ds} + L_{dr}))^2} \tag{7}$$

where

$$R_{EQ} = s\frac{sR_B + (\cos\alpha)^2 R_s + \cos\alpha\sqrt{\Gamma}}{s^2 - (\cos\alpha)^2} \tag{8}$$

$$\Gamma = (R_B + sR_s)^2 + (s^2 - \cos^2\alpha)(\omega_s(L_{ds} + L_{dr})) \tag{9}$$

$$R_B = (R_r + 0.55R_f) \tag{10}$$

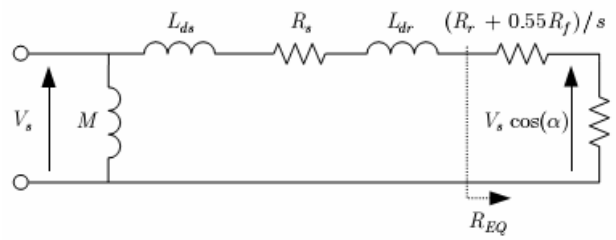

Fig. 5. Equivalent circuit of DFIG with static Kramer drive.

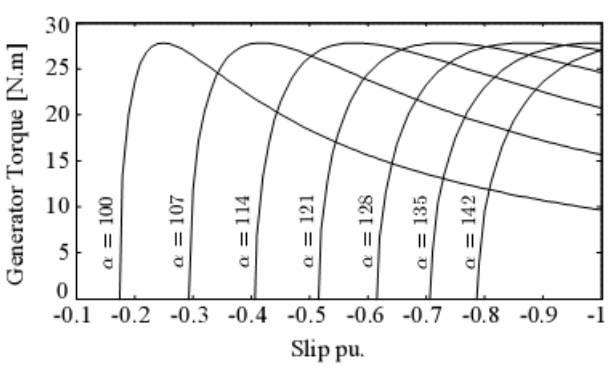

Fig. 6. Torque characteristics versus slip of a DFIG with static Kramer drive for different values of a .

Variable speed operation is achieved by controlling the firing angle of the thyristor, and hence the slip power. Figure 6 shows a plot of generator torque versus slip by varying firing angles from 100 to 142 degrees with an increment of 7 degrees. Note that the range of the firing angle a must be between 90^o and 180^o for inverting mode operation.

Electrical power output, P_E , of the DFIG is affected by its efficiency as given in (11).

$$P_E(\cos\alpha,\Omega) = \eta(\cos\alpha,\Omega)\cdot\Omega\cdot T_G(\cos\alpha,\Omega) \tag{11}$$

where

$$\eta(\cos\alpha,\Omega) = \frac{\Omega_S(1-\cos\alpha)}{\Omega} \tag{12}$$

2.3 Mathematical Model of System

The torque balance of the system is

$$T_a = J\dot{\Omega} + B\Omega + T_g \tag{13}$$

By neglecting the effects of friction and stiffness of the transmission shaft and mechanical losses, the dynamic model can be described by the following equation [10]:

$$\dot{\Omega} = f(\cos\alpha, v, \Omega) = \frac{1}{J}\cdot[T_a(\Omega, v) - T_G(\cos\alpha,\Omega)] \tag{14}$$

Figure 7 shows electrical power from the wind captured by the turbine blades versus rotational speed at 7 different wind velocities. The electrical power is limited by two boundary lines $P_E(\Omega,0)$ and $P_E(-1,\Omega)$. These two lines present the lower and upper limits of the firing angle between 90 and 180 degrees, respectively.

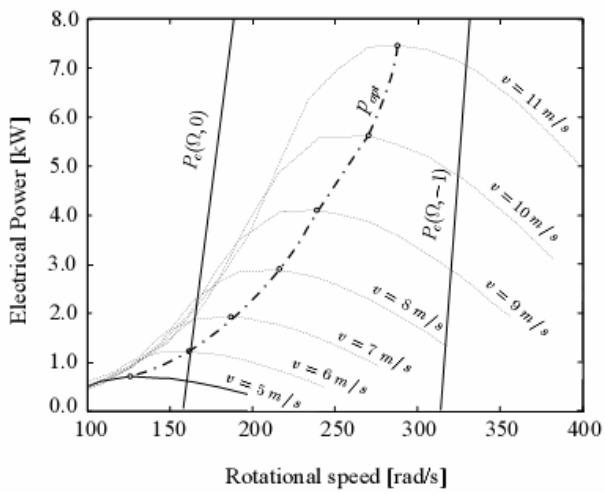

Fig. 7. Aerodynamic and generator power versus rotational speed of generator shaft for various wind velocity.

3. VARIABLE STRUCTURE CONTROL

3.1 Sliding Surface Design

For maximum peak power tracking, the sliding surface can be defined normalized power error in (15). The control objective is to drive the normalized power error to be zero [6].

$$y = h(\cos\alpha,\Omega) = \frac{P_E(\cos\alpha,\Omega)}{P_R} - 1 \tag{15}$$

Let $$u = \cos\alpha \tag{16}$$

Differentiating (15) yields:

$$\dot{y} = \frac{\partial h(u,\Omega)}{\partial u}\cdot\frac{du}{dt} + \frac{\partial h(u,\Omega)}{\partial\Omega}\cdot\frac{d\Omega}{dt} \tag{17}$$

Therefore, the following discontinuous dynamics is imposed.

$$\dot{y} = -W\cdot\mathrm{sign}(y), W > 0 \tag{18}$$

From (17), let

$$L_f h = \frac{\partial h(u,\Omega)}{\partial\Omega}\cdot\frac{d\Omega}{dt} \tag{19}$$

Substituting (19) into (17), $\dot{u}$ is calculated from

$$\dot{u} = -\left(\frac{\partial h(u,\Omega)}{\partial u}\right)^{-1}\cdot[L_f h - \dot{y}] \tag{20}$$

Substituting (18) into (20), $\dot{u}$ is calculated from

$$\dot{u} = -\left(\frac{\partial h(u,\Omega)}{\partial u}\right)^{-1}\cdot[L_f h + W\cdot sign(h(u,\Omega))] \tag{21}$$

Note that from (16) with $90^o < \alpha < 180^o$, then $-1 < u < 0$.

With (14)-(21), we can build a control block diagram of the SMC as shown in Figure 8. The SMC control enclosed by the dash line receives the rotational speed, Ω, and the wind speed, *v*, to generate the control parameter, *u*, to control the plant to achieve the control objective.

3.2 Sliding Mode Control in Stall Region

The output power captured from the wind can be limited by stall regulation. The stall effect is a phenomenon that air flow separates at the wind turbine blade's surface. The separation will limit aerodynamic power and can be controlled by the rotational speed. To stall the turbine, its operating point should be moved to the left of the $c_P^{\max}$ in Figure 3. Since the sliding surface designed by (15) has only one control objective (maximum peak power tracking), (15) is modified by adding normalized speed error to take into account power limit.

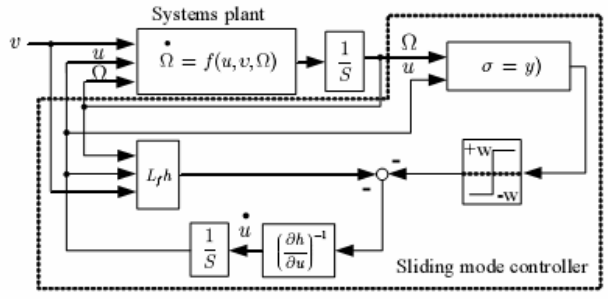

Fig. 8. Block diagram of the dynamic SM controller.

$$\sigma = y - \beta\left(\frac{\Omega}{\Omega_o} - 1\right) \tag{22}$$

$$\dot{\Omega} = \frac{\partial h(u,\Omega)}{\partial u}\cdot\frac{du}{dt} + \left[\frac{\partial h(u,\Omega)}{\partial \Omega} - \frac{\partial \beta\left(\frac{\Omega}{\Omega_o} - 1\right)}{\partial \Omega}\right]\cdot\frac{d\Omega}{dt} \tag{23}$$

Therefore, the following discontinuous dynamics is imposed.

$$\dot{\sigma} = -W \cdot \mathrm{sign}(\sigma), W > 0 \tag{24}$$

From (24), let

$$L_f q = \left[\frac{\partial h(u,\Omega)}{\partial \Omega} - \frac{\beta}{\Omega_o}\right]\cdot\frac{d\Omega}{dt} \tag{25}$$

Substituting (25) into (23), $\dot{u}$ is calculated from

$$\dot{u} = -\left(\frac{\partial h(u,\Omega)}{\partial u}\right)^{-1}\cdot\left[L_f q - \dot{\sigma}\right] \tag{26}$$

Substituting (25) into (23), $\dot{u}$ is calculated from

$$\dot{u} = -\left(\frac{\partial h(u,\Omega)}{\partial u}\right)^{-1}\cdot\left[L_f q + W\cdot sign(\sigma)\right] \tag{27}$$

In order to assure local stability of the closed loop sliding dynamics to any equilibrium point in the stall region, it is sufficient to choose a gain, *b* , satisfying: [6]

$$\beta > \max_{\lambda}(\chi(\lambda)) \tag{28}$$

where

$$\chi(\lambda) = \frac{dC_p(\lambda)}{d\lambda}\cdot\frac{\lambda}{C_p(\lambda)} \tag{29}$$

The coefficient $\chi(\lambda)$ is negative in the normal operating region, positive in the stall region and zero at λ_0.

4. CASE STUDY

4.1 Simulation System

A 7.5 kW wind energy conversion system using a DFIG with a static Kramer drive is considered in simulations (relevant parameters given in appendix). The simulations are based on the control box diagram in Figure 8.

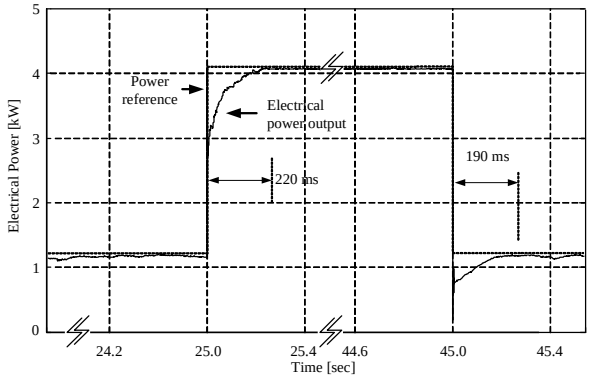

Fig. 9. Dynamic response of maximum peak power tracking to step wind speed.

4.2 Dynamic Response of Maximum Peak Power Tracking

This simulation starts by keeping a wind speed constant at 6 m/s until t = 25 s. The wind speed is then stepped-up to 9 m/s until t = 45 s, and stepped-down to 6 m/s again. The simulation result is shown in Figure 9. We can see that when the wind speed is stepped-up, the SMC uses 220 ms to track the maximum power, and when wind speed is stepped-down, the SMC takes 190 ms to reach the maximum power.

4.3 Maximum Peak Power Tracking without Power Limit

The SM controller uses the sliding surface defined in (15) without power limit. The input wind speed shown in Figure 10 (a) with a power reference from (3). The output power shown in Figure 10 (b), and Figure 10 (c)

is the error between the reference power and output power. Conversely, when the wind speed is greater than 9 m/s, the input power from the wind increases. From Figure 10, if the wind speed is increased at t = 52 s, the output power will be limited owing to $\cos a = 180^{o}$. The corresponding power coefficient and tip speed ratio are shown in Figures 11 (a) and (b), respectively. These figures can confirm that before t = 35 s, c_P is controlled at the maximum value until the wind speed is lower than 5 m/s (35s < t < 52s) During such a period, c_P is not maximum because of the lower limitation of the firing angle (on the left hand side in Figure 7).

4.4 Maximum Peak Power Tracking with Power Limit

This section simulates the sliding surface defined (22). In this mode the wind turbine operates with small values of c_P to limit the input from the wind. Figures 12 (a) and (b) show the input wind speed and output power respectively. The corresponding power coefficient and tip speed ratio are shown in Figures 13 (a) and (b), respectively. In this case, the power is limited at 4 kW (rated wind speed of 9 m/s). It is clearly seen that when the wind speed is lower than 9 m/s, the output power is maximum. Conversely, if the wind speed is higher than 9 m/s, the output power will be limited at 4 kW. The control trajectory with power limit by the SMC is shown in Figure 14.

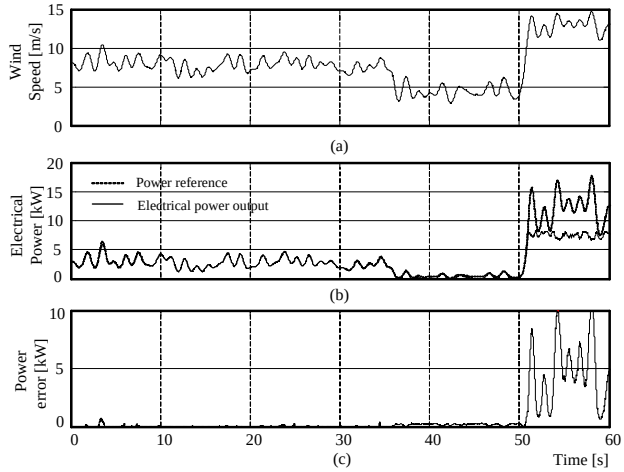

Fig. 10. a) Wind speed, b) Reference and output power, c) Power error.

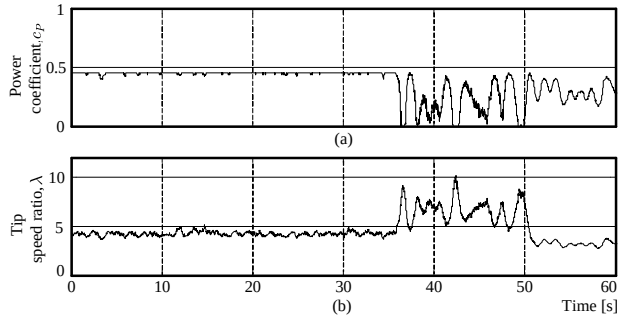

Fig. 11. a) Power coefficient, b) Tip speed ratio.

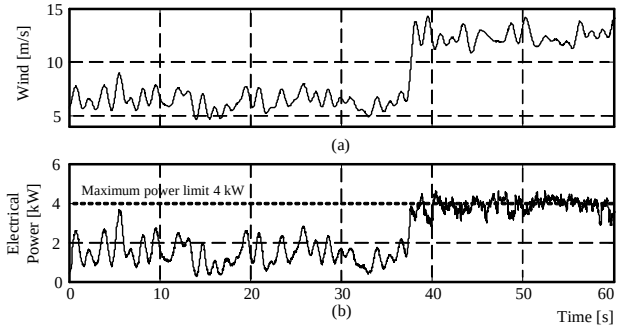

Fig. 12. a) Below rated and above rated wind speed, b) Output power with power limit at 4kW.

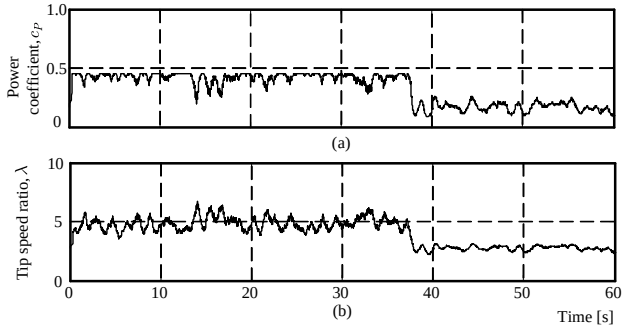

Fig. 13. a) Power coefficient, b) Tip speed ratio at 4kW.

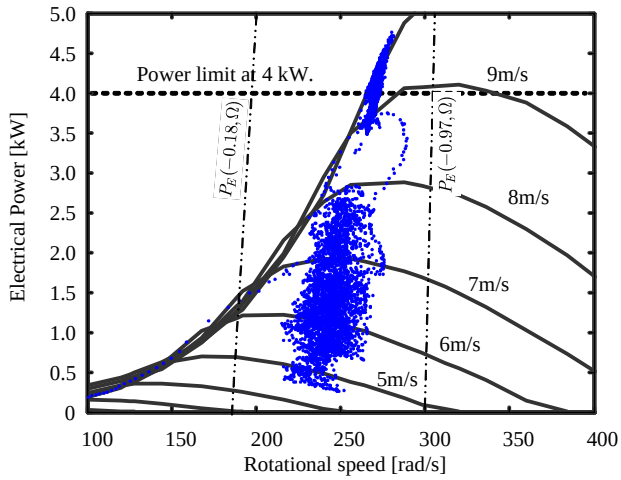

Fig. 14. Output power trajectory with stall regulation.

NOMENCLATURE

ρ	air density
λ	tip speed ratio
λ_O	tip speed ratio at maximum c_P
λ_l	tip speed ratio at low speed side
λ_h	tip speed ratio at high speed side
c_T	torque coefficient
c_P	power coefficient
$c_P^{\max}$	maximum power coefficient

A	area of turbine blade move in the air
v	velocity speed of wind
Ω	rotational speed of rotor
Ω_s	mechanical synchronous speed
Ω_o	the rotational speed at the operation point
ω_s	electrical synchronous speed
V_s	stator line voltage
R_S	stator resistance
R_R	rotor resistance
R_F	DC link resistance
L_{ds}, L_{dr}	*d*-axis stator and rotor leakage inductance
s	Slip per unit
α	firing angle
J	moment of inertia
T_g	generator torque
T_a	aerodynamic torque
η	power efficiency
P_E	electrical power output from generator
P_G	mechanical power input from turbine
u	cosine of firing angle
P_R	command reference power
β	positive constant gain

REFERENCES

[1] Çadirci I. and Ermiş, M. 1992. Double-output induction generator operating at subsynchronous and supersynchronous speeds: steady-state performance optimization and wind-energy recovery. *IEE Proc. C*, 139(5): 429-442.

[2] de Battista, H., Puleston, P., Mantz, R, and Christainsen, C. 2000. Sliding mode control of wind energy systems with doig: Power efficiency and torsional dynamics optimization. *IEEE Trans. Power Syst*., 15(2): 728-734.

[3] Hoffmann, R. and Mutschler, P. 2000. The Influence of Control Strategies on the Energy Capture of Wind Turbines. *IEEE Trans. Ind. App*, 2: 886–893.

[4] Thriringer, T. and Linders, J. 1993. Control by Variable Rotor Speed of a Fixed-Pitch Wind Turbine Operating in a Wide Speed Range. *IEEE Trans. Energy Con.*, 8(3): 520–526.

[5] Manwell, J.F., McGowan, J.G. and Rogers, A.L. 2004. *Wind Energy Explained*, John Wiley & Sons, West Sussex, England.

[6] de Battista, H. and Mantz, R. 2004. Dynamical variable structure controller for power regulation of wind energy conversion systems. *IEEE Trans. Energy Conv*., 19(4): 756-763.

[7] Utkin, V., Guldner, J. and Shi, J. 1999. *Sliding Mode Control in Electromechanical Systems*. London, U.K.: Taylor & Francis.

[8] Itkis, U. 1976. *Control systems of variable structure*, New York.: John Wiley & Sons.

[9] Sira-Ramirez, H. On the dynamical sliding mode control of nonlinear systems. *Int. Journal of Control*, 57(5): 1039-1061.

[10] Gopalswamy, S. and Hedrick, J.K. 1993. Tracking nonlinear non minimum phase systems using sliding control. *Int. Journal of Control*, 57(5): 1141-1158.

[11] Bose, B.K. 2001. *Modern Power Electronics and AC Drives.* Prentice Hall.

[12] Dewan, S.B., Slemon, G.R. and Straughen, A. 1984. *Power Semiconductor Drives*, John Wiley & Sons.

APPENDIX

The parameters used in simulation are provided below:

V_s	380 V
R_s	$400\,m\Omega$
R_r	$200\,m\Omega$
R_f	$10\,m\Omega$
L_{ds}	$122\,m\Omega$
L_{dr}	$37\,m\Omega$
J	7.5 Kg m^2
ρ	1.26kg/m^3
λ_O	4.5
$c_p^{\max}$	0.455
A	19.6350m^2